AGU PUBLICATIONS

JGR

Journal of Geophysical Research: Oceans

RESEARCH ARTICLE

10.1002/2017JC013148

Special Section:
Sea State and Boundary Layer Physics of the Emerging Arctic Ocean

Key Points:

- New methodology to retrieve wave parameters in the marginal ice zone (MIZ) from full polarization synthetic aperture radar (SAR) imagery
- Method to derive wave attenuation rates within the MIZ from quad-polarization SAR imagery was developed and verified with in situ data
- Observed wave direction shifting and wavelength changes in the MIZ and validation with a modern wave attenuation model

Correspondence to:
W. Perrie,
william.perrie@dfo-mpo.gc.ca;
H. Shen,
Hui.Shen@dfo-mpo.gc.ca

Citation:
Shen, H., Perrie, W., Hu, Y., & He, Y. (2018). Remote sensing of waves propagating in the marginal ice zone by SAR. *Journal of Geophysical Research: Oceans*, *123*, 189–200. https://doi.org/10.1002/2017JC013148

Received 2 JUN 2017
Accepted 18 DEC 2017
Accepted article online 27 DEC 2017
Published online 10 JAN 2018

© 2017. American Geophysical Union. All Rights Reserved.

Remote Sensing of Waves Propagating in the Marginal Ice Zone by SAR

Hui Shen[1], William Perrie[1], Yongcun Hu[1], and Yijun He[2]

[1]Ocean and Ecosystem Sciences Division, Bedford Institute of Oceanography, Dartmouth, NS, Canada, [2]School of Marine Sciences, Nanjing University of Information Science and Technology, Nanjing, China

Abstract Wave-ice interactions are important in high sea state conditions, when waves propagate from the open ocean into the marginal ice zone (MIZ) and the pack ice. In situ observations of waves and wave-ice interactions can be obtained at a small number of MIZ locations in costly and challenging experiments, whereas remote sensing using satellite RADARSAT-2 SAR (synthetic aperture radar) images can observe waves throughout the MIZ, in all weather conditions. We present a methodology to retrieve MIZ wave parameters from *polarimetric* SAR data. As an application, we describe the characteristics of waves propagating from open water into the MIZ, as generated by a strong low pressure system that developed to the east of Greenland. As waves penetrate the MIZ, SAR remote sensing observations suggest *increased* dominant wavelengths, *attenuated* wave energy and *shifted* mean wave directions. The SAR observations and estimates for retrieved wave attenuation in the MIZ are shown to be consistent with wave attenuation theory and in situ field observations. Thus, valuable estimates of MIZ waves over large spatial scales at high-resolution are provided by the SAR measurements.

1. Introduction

Arctic is experiencing dramatic sea ice reductions in recent years. According to the National Snow and Ice Data Centre (NSIDC), the maximum extent of Arctic sea ice is experiencing a record low in 2017 for the third straight year in the entire 38 year satellite record. Looking to the future, climate change projections suggest ice free summers in the Arctic by the late 2030s (Wang & Overland, 2009). The emergence of increasingly open waters during Arctic summers suggests new opportunities such as the opening of the Northern Sea Route and the Northwest Passage and energy-related exploration in Arctic coastal areas. Environmental factors associated with reductions in sea ice include increasingly severe storms and higher waves, due to increased winds and longer wave fetches (Khon et al., 2014), with associated risks to a fragile ecosystem, hazards such as oil spills and potential environmental damage.

The MIZ is highly dynamic with coupled interactions between the ice floes and open ocean processes; it is a part of the seasonal ice zone that varies in width (100 to 200 km) that extends from the ice edge into the ice pack, where waves and swells affect the ice. With more open water in summers in the Arctic, waves are increasingly important for Arctic Ocean dynamics. Moreover, MIZ wave-ice interactions have a potentially important role in the break-up and rapid retreat of the sea ice, in both the Arctic Ocean and the Southern Ocean, particularly with the increasing wave heights experienced over the last couple of decades as the Arctic ice extent decreases (Kohout et al., 2014; Stopa et al., 2016; Thomson & Rogers, 2014). Moreover, wave propagation from open ocean water into the MIZ is modified by the wave scattering and attenuation that occurs, which strongly depends on the properties of the ice floes (Squire & Montiel, 2016). However, present operational wave models, such as WAVEWATCHII (hereafter WW3) (Tolman, 2009), include incomplete parameterizations for MIZ wave scattering and attenuation among pancake ice.

A parameterization for wave-ice interactions and wave scattering was developed by Perrie and Hu (1996) and Meylan and Masson (2006), taking into account the energy transfers within the wave spectra and between waves and the ice floes, as the waves propagate through the MIZ. This formulation tries to account for ice floe motions, as generated by the waves, and is dependent on ice floe thickness, ice concentration, floe lengths, and wave characteristics like frequency and wave age. Several in situ field experiments have recently been completed. These include the recent Antarctic MIZ experiment by Kohout et al. (2014), the

MIZ experiment in the Beaufort Sea (Lee et al., 2012) and the Sea State Boundary Layer experiment, also in the Beaufort Sea in 2015 (Thomson et al., 2013). These activities follow earlier experiments (for example, Wadhams et al., 1988). Related studies have looked at wave scattering and attenuation in interactions between waves and ice floes (Kohout & Meylan, 2008; Kohout et al., 2014; Montiel et al., 2016). Recent efforts to model waves in the MIZ have highlighted the correspondence between sea ice categories and wave dissipation rates (Rogers et al., 2016).

Remote sensing is an important method to collect quantitative information about sea ice. For example, multibeam lidar (Sutherland & Gascard, 2016) and SAR (synthetic aperture radar) are capable of wave measurements in ice covered areas. The focus of the present study is wave scattering and attenuation by ice floes as revealed by SAR observations. The theory of ocean wave imaging in open water by SAR has been well developed and recognized (e.g., Alpers et al., 1981; Hasselmann et al., 1985). For long waves in small patches of thin ice (compared to wavelength), Vachon et al. (1993) showed that the traditional theory for wave imaging still holds; which is confirmed by Schulz-Stellenfleth and Lehner (2002), who presented detailed theoretical analysis on damping of ocean waves by sea ice based on ERS-2 SAR data. Liu et al. (1992) used airborne SAR data to study wave attenuation in the MIZ during the Labrador Ice Margin Experiment (LIMEX); Wadhams et al. (2002) studied wave dispersion relationship in frazil-pancake ice zone by ERS SAR data. Recent studies suggest that waves experience no obvious dispersion changes in going from open water into the MIZ (Rogers et al., 2016).

The advent of a new generation of operational SAR satellites, such as RADARSAT-2, TerraSAR-X and Sentinel-1, with *multi-polarizations* and high-spatial resolutions, has generated new opportunities for studies of wave-ice interactions in the MIZ. Recently, Ardhuin et al. (2017) made a detailed investigation of the unique velocity bunching mechanism of *single polarization* SAR wave imaging in a fully ice covered area and developed a new methodology for wave parameter retrievals based on Sentinel SAR data. Gebhardt et al. (2016) studied waves propagating into the MIZ during the same storm system that we consider in this present study, based on X band TerraSAR data, obtained 2 days after our C band RADARSAT-2 SAR measurements. They found that the wave dispersion effect due to the long distance traveled from the storm generation site can account for the wavelength changes in their SAR imagery. Here, we present a study of the wave-ice interactions in marginal ice zone, based on polarimetric RADARSAT-2 SAR data analysis and theoretical model simulations.

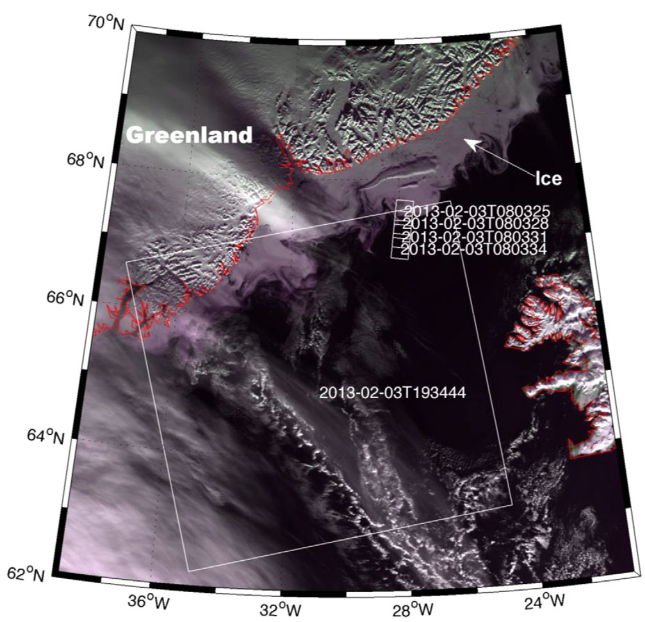

Figure 1. Spatial coverage of the RADARSAT-2 ScanSAR and quad-pol SAR images in 3 February 2013 overlaying a MODIS image showing ice conditions off the coast of Greenland (Modis image time: 5 February 2013 16:24:03UTC).

2. Data and Methods

2.1. Data

On 3 February 2013, a strong low pressure system dominated the southeast region of Greenland with the central low pressure reaching 950 hPa. It propagated eastward generating strong winds and high waves. RADARSAT-2 SAR images were acquired covering this event, including a ScanSAR mode image with 50 m resolution and 500 km $\times$ 500 km coverage, as well as quad-polarization (pol) fine mode SAR images, with 4.7 m pixel resolution and 25 km $\times$ 25 km spatial coverage per frame. The coverage of these images is shown in Figure 1, off the southeast coast of Greenland. A single MODIS image was also obtained at the same location on 5 February 2013, providing sea ice observations at approximately the same time as the SAR imagery (Figure 1).

Wave height measurements derived from altimeter data from Jason-2 are utilized for wave analysis in the open ocean and for validation of retrieved wave parameters from the SAR data. As shown in Figure 1c, significant wave heights up to 8 meters were observed by the altimeter in the open ocean region of the study area.

ECMWF ERA-Interim wave reanalysis products are used to demonstrate the general wave patterns in the studied area. Figures 2a and 2b show the spatial distributions of wind wave and swell during the

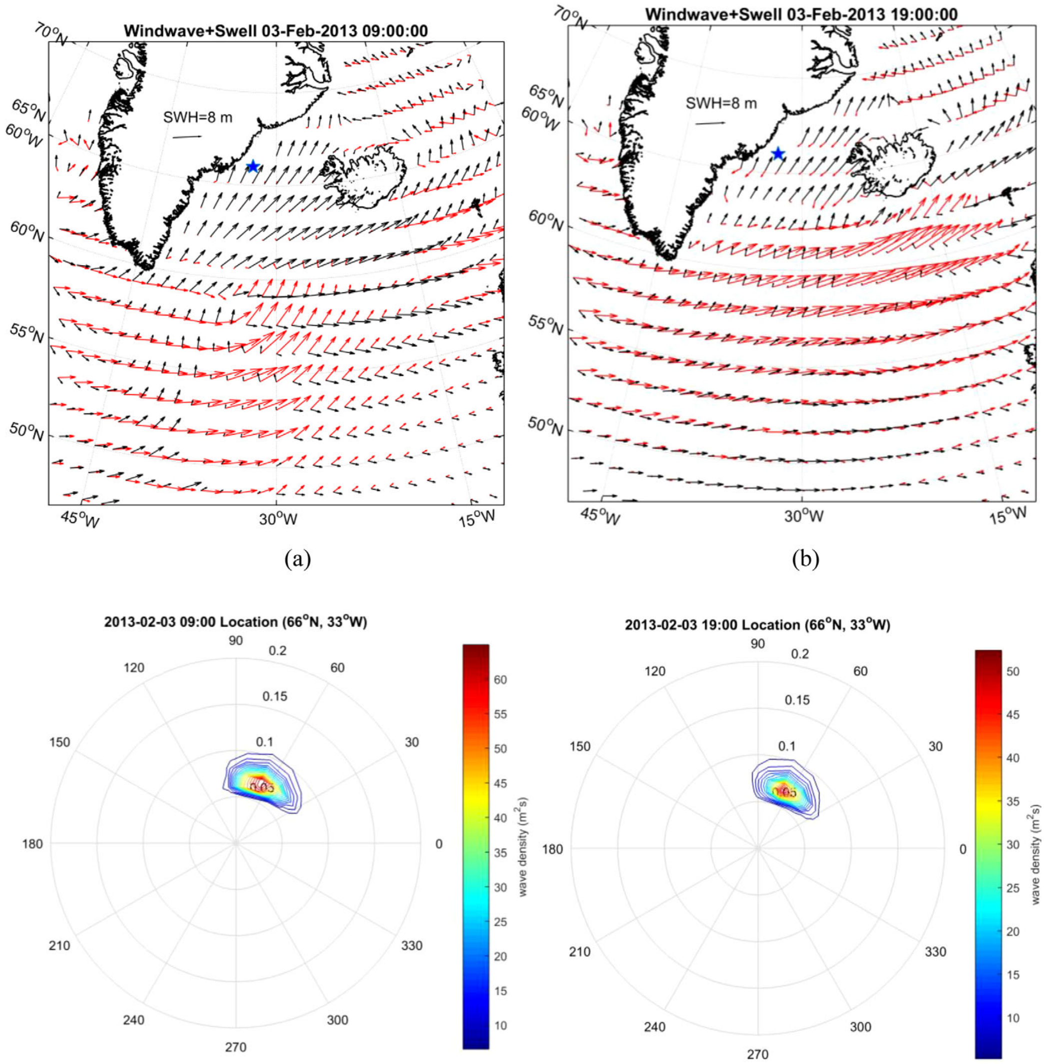

(c)

Figure 2. Wind waves (red arrows) and swell (black arrows) at 09:00 (a) and 19:00 (b), 3 February 2013 from ECMWF interim reanalysis data. (c) Wave spectrum before the ice edge in position (66°N, 33°W), is marked as blue star in Figure 2b. Units of radial wavenumber axis are m^{-1}.

RADARSAT-2 SAR imaging times. In the vicinity of the SAR observation area, near the ice edge, the ECMWF data show a pure swell system at 09:00 3 February 2013 when the quad-polarization RADARSAT-2 SAR images were taken and a dominant swell system at 19:00 3 February 2013 when the ScanSAR image was measured (Figure 2c). The strong swell waves penetrate into the marginal ice zone before reaching the packed ice near the coast, providing a unique opportunity to study the wave-ice interactions in the MIZ.

2.2. Method Wave Retrievals

This study focuses on wave retrievals from the MIZ. To obtain wave parameters from satellite data, the ocean surface medium in the image needs to be homogeneous, to avoid spurious signals in the wave spectrum analysis (He et al., 2006). Any potential inhomogeneity of the ice field may lead to spurious high frequency signals in the image, and causing uncertainties in the SAR retrieval fields. Efforts have to be made at the image preprocessing stage to minimize this effect; for example, carefully choosing image blocks without apparent ice signatures, such as ice ridges, ice leakage and application of image enhancing techniques such as de-trending, smoothing etc. The first step in the retrieval process is to discriminate sea ice from the open water. In operational sea ice analyses using single-pol ScanSAR images, ice discrimination generally

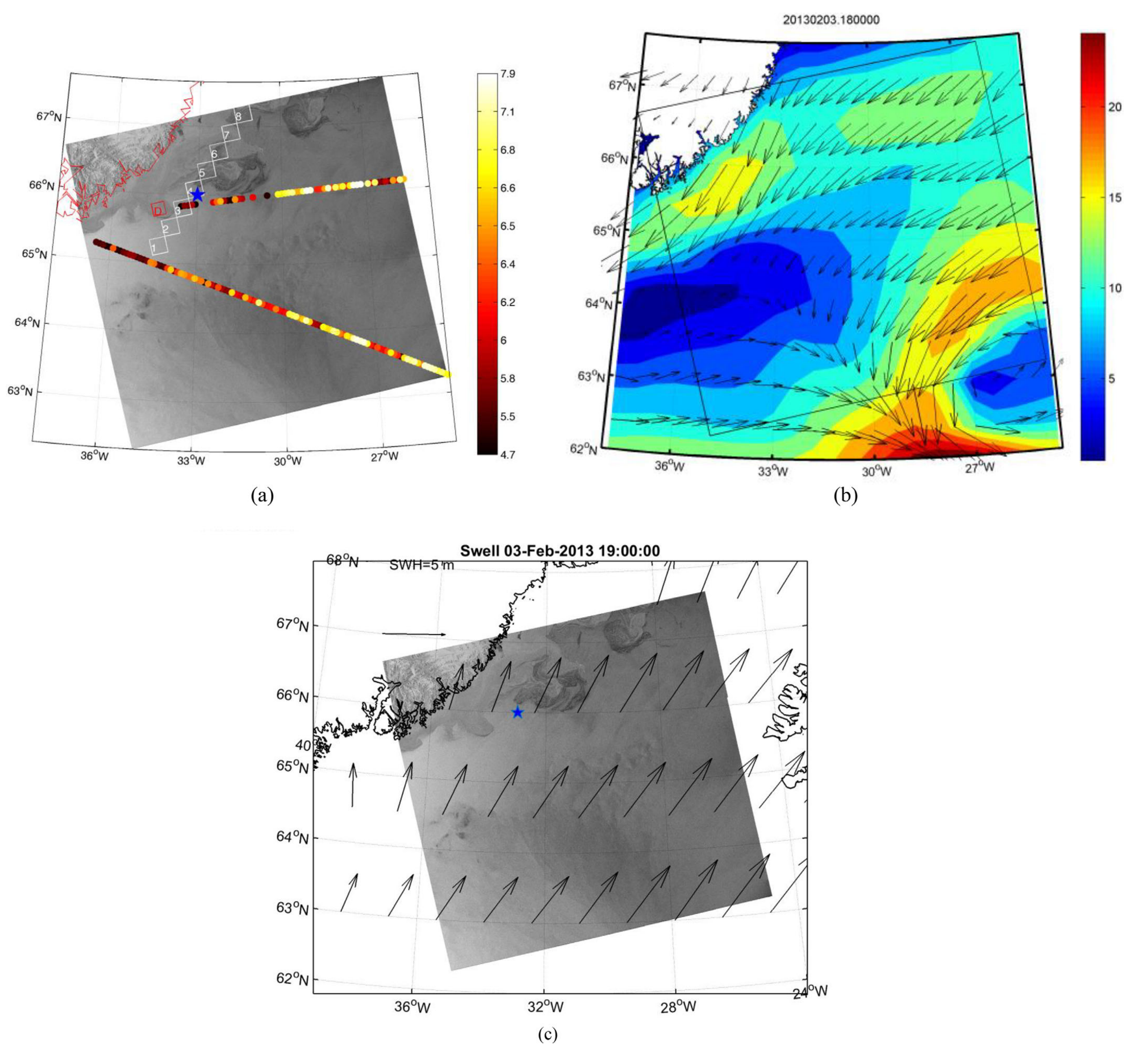

Figure 3. RADARSAT ScanSAR image at 19:44UTC 3 February 2013 overlaid by (a) significant wave height (unit: m) from Jason-2 altimeter in (a). White boxes represent transect along the wave direction; box "D" is used in Figure 4. Blue star is the location used in Figure 2. (b) Local wind field from CMC model (unit: m/s). (c) Significant wave height and direction for swell from ECMWF data.

involves manual interpretation by an experienced forecaster, relying on the different textures of ice compared to those of open water in the images. For full polarization quad-pol RADARSAT-2 SAR images, the combination of both phase and amplitude information from the SAR measurements, in different polarizations, may contribute information to enhance the skill of the forecaster in discriminating ice from open water.

Image spectra from SAR measurements are retrieved based on spectral analysis, using the two- dimensional Fast Fourier Transform. For ScanSAR images, a linear modulation transfer function MTF is used for this particular case at 19:44 on February 3 (Figure 3a). The applicability of linear MTF for the ScanSAR image analysis will be discussed in detail. For quad-pol SAR measurements (Figure 8), the method to retrieve wave spectra from image spectra is adapted from He et al. (2006), which was originally developed for AirSAR data and later validated with RADARSAT-2 quad-pol data (Zhang et al., 2010). This approach is based on the theoretical relationship between fully polarimetric SAR data and wave slope spectrum. In this approach, a modulation transfer function (MTF) is *not* required. The MTF approach is a relatively complicated nonlinear formulation for retrieval of high sea-state wind waves, whereby tilt, hydrodynamic and velocity bunching modulations are responsible for wave stipes shown in SAR intensity images (Alpers et al., 1981). For waves within ice, Schulz-Stellenfleth and Lehner (2002) provided detailed theoretical analysis to justify the capability of wave retrieval from SAR imagery. Velocity bunching is a mechanism by which swell and windsea are evident in SAR images especially in the azimuthal (platform moving) direction. An innovative methodology to retrieval wave information from ice area by taking advantage of the velocity bunching mechanism is presented by Ardhuin et al. (2017). They derive the orbital velocity by fitting the velocity bunching theory to the wave shapes presented in SAR image; only single polarization SAR data are needed. Both Ardhiun et al. (2017) and He et al. (2006) do not rely on the explicit form of the MTF.

Conventionally, the image spectra and wave spectra are connected by a modulation transfer function (Bendat & Piersol, 1971) expressed as,

$$P(k) = |R^{SAR}(k)|^2 P_{\xi}(k) \tag{1}$$

where $P(k)$ and $P(k)$ are the image intensity spectrum and the ocean wave height spectrum, respectively and R is the modulation transfer function (MTF).

In order to obtain the dissipation rate of the waves, it is necessary to estimate the wave spectrum from the image spectrum. Under linear conditions, the MTF is a superposition of the tilt, hydrodynamic and velocity bunching functions. When MTF is a linear formula, the attenuation rate for the wave spectra can be directly obtained from the image spectra (Liu et al., 1992), which is a valid assumption for swell or low amplitude wind waves. Indeed, studies show that the MTF is a linear sum of tilt and hydrodynamic modulations for Real Aperture Radar (RAR). However, for SAR the velocity bunching mechanism provides a nonlinear contribution to the modulation (Alpers et al., 1981). The nonlinear effect is reduced for swell or for waves propagating along the radar look (range) direction.

To estimate the nonlinearity of MTF, Alpers et al. (1981) proposed a formula (2) to calculate the nonlinearity coefficient. The ECMWF data in Figure 2 already suggest that the wave system in this study is a dominantly swell. It is interesting to see how the nonlinearity coefficient works in this case. With 3 m significant wave heights at the edge of the MIZ area, as suggested by Jason-2 altimeter measurements, equation (2) suggests that the nonlinear coefficient is 0.3, which can be considered a linear velocity bunching mechanism (Alpers et al., 1981; Brüning et al., 1994). Therefore, the wave attenuation rate coefficient can be directly obtained from the image spectrum derived from the ScanSAR image, following Liu et al. (1992),

$$C = \frac{R}{4V} g^{1/2} K_p^{3/2} H_s \cos\vartheta \cos\phi_p \tag{2}$$

where g is the gravitational acceleration, R is the target range, V is the platform velocity, K_p and ϕ_p are the peak wave component and its propagation direction relative to azimuth, ϑ is radar incidence angle and H_s is the significant wave height.

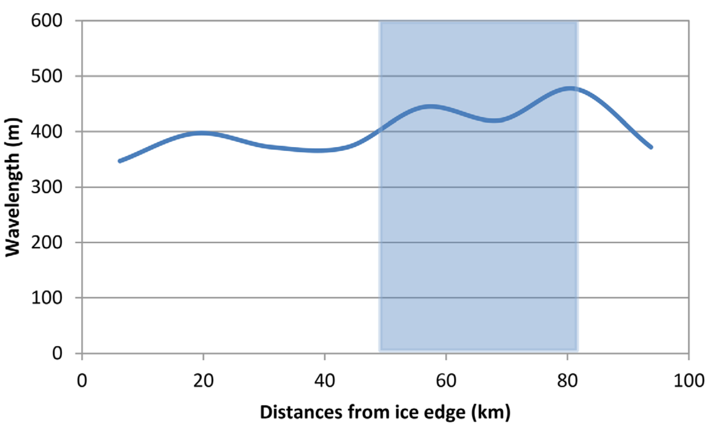

Figure 4. Peak wavelength changes as derived from SAR imagery along transect labeled by boxes 1 to 8 in Figure 3. Shaded area denotes the MIZ.

3. Wave Propagation Through Ice in the MIZ

In winter, Greenland is typically surrounded by pack ice. The MIZ separates the open water and the pack ice and is composed of ice floes of various ice characteristics and properties. The RADARSAT-2 SAR measurements shown here suggest that the wave stripes are still present 200 km from the ice edge along the transect indicated in Figure 3. As waves propagate through the MIZ, wave energy suffers attenuation and dissipation by scattering interactions and momentum transfer to the ice floes (Doble & Bidlot, 2013; Kohout et al, 2014; Meylan & Masson, 2006; Perrie & Hu, 1996; Toffoli et al., 2015; Wadhams, 1986). Energy transferred from the waves contributes to ice floe motions.

The effects of these processes on wave attenuation and scattering can be estimated by in situ measurements (Kohout et al., 2014; Meylan et al., 2014). Our objective is to derive these estimates from remotely sensed SAR imagery.

3.1. Wave Length Changes in MIZ

As mentioned above, the waves generated by the large synoptic-scale low pressure system were observed by altimeter measurements from Jason-2 and estimated to have significant wave heights up to 8.0 m in the open ocean (Figure 3). ASCAT scatterometer measurements and ECMWF wind data suggest that the wind direction at the center of the storm is generally to the east, with wind speeds in the range of 25–30 m/s, generating strong swells propagating to the north toward the studied area. In the area covered by the SAR imagery, local winds are also present along the coast, but blowing to the southwest, with speeds of about 10 m/s, as indicated by the high resolution regional CMC (Canadian Meteorological Centre) model (Figure 3b). If fully developed, these waves can have wavelengths of up to 95 m, assuming equilibrium wave relations (Pierson & Moskowitz, 1964). Analysis of the spectrum from the SAR observations along the transect (Figure 3) shows pure swell, with no local wind –generated waves. This result is consistent with the ECMWF data shown in Figure 2. In a different location which is ~200 km away further north, Gebhardt et al. (2016) investigated two wave systems in their TerraSAR X images; ECMWF data suggest that the additional wind wave system corresponds to the open wind fetches which favors wave development traveling from open water into ice (Figure 2). In the area of present study, the wind fetch is limited by ice since local wind direction is off ice.

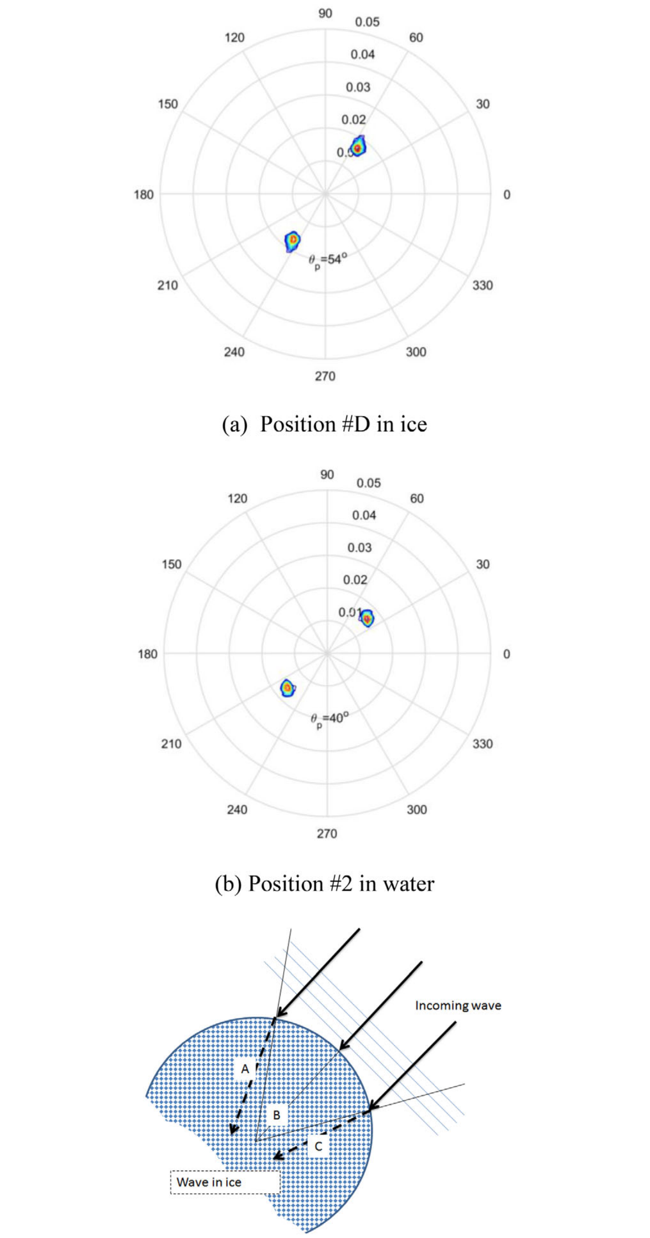

(a) Position #D in ice

(b) Position #2 in water

(c) Schematic illustration of wave refraction due to changed medium

Figure 5. Wave direction shifts of box #D (Figure 1c) in the ice zone as compared to open water box #2. A, B, C are used to demonstrate locations with different refraction wave direction.

The ScanSAR image was partitioned into sub-images, each of 512 × 512 pixels, in order to obtain the wave transformation patterns, as the waves propagate from open water *through the ice floes of the MIZ*. Corresponding image spectra were obtained for each of the sub-images. Spectral analysis shows that waves are propagating from the northeast to the southwest, in the ScanSAR image. As shown in Figure 3, a transect along the wave direction is chosen for further analysis. The transect includes locations in open water, in the MIZ and on the other side of the ice region, in open water again.

In the open water (box #1, as indicated), the dominant wavelength is 339 m (Figure 4); the deep water dispersion relation suggests a corresponding wave period of 14.9 s. Along the transect defined by boxes 1 to 8 in Figure 3, variations in the peak wavelength within the ice are evident (Figure 4), with increasing peak wavelengths, from boxes #5 to #7, when MIZ ice is present along the transect path. From boxes #7 to #8, the wavelength decreased, as waves continue to propagate, back into open water. The lengthening of the peak wavelengths in the MIZ is consistent with our general understanding that ice floes and related ice material tend to act as a low frequency filter for the ocean waves (Collins et al., 2015), whereby high frequency wave energy is dissipated and scattered. As suggested by Sutherland and Gascard (2016), both viscous dissipation and scattering mechanisms are important in the MIZ, as both mechanisms can be used in the overall interpretation of MIZ wave attenuation. In section 3, viscosity and scattering models are applied to simulate and explain the wave attenuation detected by the SAR image. SAR observations indicated decreased wavelength when waves propagate out of ice back into water (Figure 4). This is likely caused by swell dissipation because in this case, swell is dominant in the front of ice tongue (Figure 2), and local wind is blowing in the *opposite* direction to incident swells (see the CMC winds in Figure 3b); when swell travels out of ice, it suffers suppression from winds, causing dissipation to the swell energy and resulting in decreased wavelengths. Note that swell dissipation *per se* is included in the recent version of WW3 model (WaveWatch Manuel v5.16).

3.2. Shift of Wave Direction

When waves propagate from open water into the MIZ, we find that changes in the dominant wave direction occur, based on a spectral analysis of the SAR images (Box #2 as compared to #D). Moreover, the wave direction shifts toward the normal direction relative to the ice edge. This can be motivated by Snell's Law which also happens when light propagates from air into water. In this case, the ice edge has approximately a circular arc shape, and the waves are propagating to the northeast direction in the water (box #2), shifted counterclockwise, toward the normal direction in the middle of the arc (Figures 5a–5c for details). In Figure 5c, we demonstrate that waves from both quadrants of the normal direction are refracted toward their respective local normal directions in the MIZ, resulting in wave convergence within the MIZ. This convergence can potentially lead to a region of enhanced wave energy accumulation, which may play a role in breaking ice floes in this area of the MIZ. Previous studies on the effects of waves on packed ice floes have suggested that a convergence of wave trains can lead to ice pack break-up and dissipation of the waves (Dumont et al., 2011; Kohout et al., 2016; Liu et al., 1992; Montiel et al., 2016; Williams et al., 2013a, 2013b). In actual ocean conditions, the shape of the ice edge is possibly often very complicated with small scale variations as compared to the wavelength. We note that such small scale variations are unlikely to cause significant impact on waves, especially if the ice thickness at the edge of the MIZ is relatively thin. Therefore, in this approach, the normal direction at the ice edge, with regard to wave refraction, refers to ice boundary curvatures larger than the dominant wavelength of the incoming waves.

3.3. Simulation Based on Wave Attenuation Theory

In literature, there are two kinds of attenuation models that are widely used to simulate wave attenuation due to the presence of ice floes, the viscous layer model and the wave scattering model. The viscous layer model considers ice cover to be continuum, whose deformation is governed by its constitutive behavior (Cheng et al., 2017). The scattering model considers the scattering effect of discrete ice floes, and wave energy transferred to ice floes by the excitation of heave, pitch and roll oscillation modes (Montiel & Squire, 2017; Perrie & Hu, 1996; many others). Although the physics behind these two category models are quite different, both models can suggest an exponential wave dissipation rate under the influence of sea ice.

The focus of our paper is not about the physical mechanisms *per se* of wave attenuation within the marginal ice zone, or about the detailed further development of these specific models. Rather, our focus is to show how SAR can help to interpret the wave attenuation *per se* within the MIZ through the following analysis.

3.3.1. Viscous Layer Model

For the viscous layer model, wave energy attenuation in sea ice is represented in the form of an exponential decay function (e.g., Sutherland & Gascard, 2016). The decay rate is quantified in terms of the fetch $X_{ice}(L;\theta)$ within the MIZ, multiplied by a wavenumber dependent attenuation coefficient $\alpha(k)=\left(v_{eff}^{0.5}k^{7/4}\right)/\left(\sqrt{2}g^{0.25}\right)$, where the effective viscosity is $v_{eff}=6.4\times10^{-4}\ m^2/s$, as derived by fitting the wave spectra parametrizations to data observed by airborne lidar measurements by Sutherland and Gascard (2016). It should be noted that the effective viscosity is dependent on the ice conditions (Rogers et al., 2016).

For simplicity, we assume that the MIZ has a linear ice edge (as shown in Figure 6), with incoming waves that are 45° to the normal direction of the ice edge. Therefore, the fetch over the MIZ ice is $X_{ice}(L;\theta)=L/sin(\theta)$ where L is the shortest distance from a given position in the ice, to the ice edge, and θ is the incoming wave direction. In this simulation, the incoming wave directional spectrum is assumed to be described by the DHH wave spectral parameterization (Donelan et al., 1985) with 8 m/s wind speed (Figure 6b).

Figures 6c and 6d show wave spectra at locations 2 km and 4 km inside the ice (positions A and B in Figure 6a), where the wave direction at the peak wave energy θ_p is shifted from the incident direction toward the normal direction, inside the ice. The shift is about 1° every km, and the associated *peak* wavenumber k_p decreases from 10.7% at 2 km to 17.5% at 4 km respectively. The model follows the SAR observations, regarding the directional shift and the changes in the *peak* wavelengths due to the attenuation. For assumed homogeneous ice conditions, the model also suggests that when the waves propagate further into the ice, the rate of directional shift decelerates and the wavelength changes continue; these effects are enhanced for higher ice concentration conditions further inside the MIZ. Wave attenuation in the MIZ also

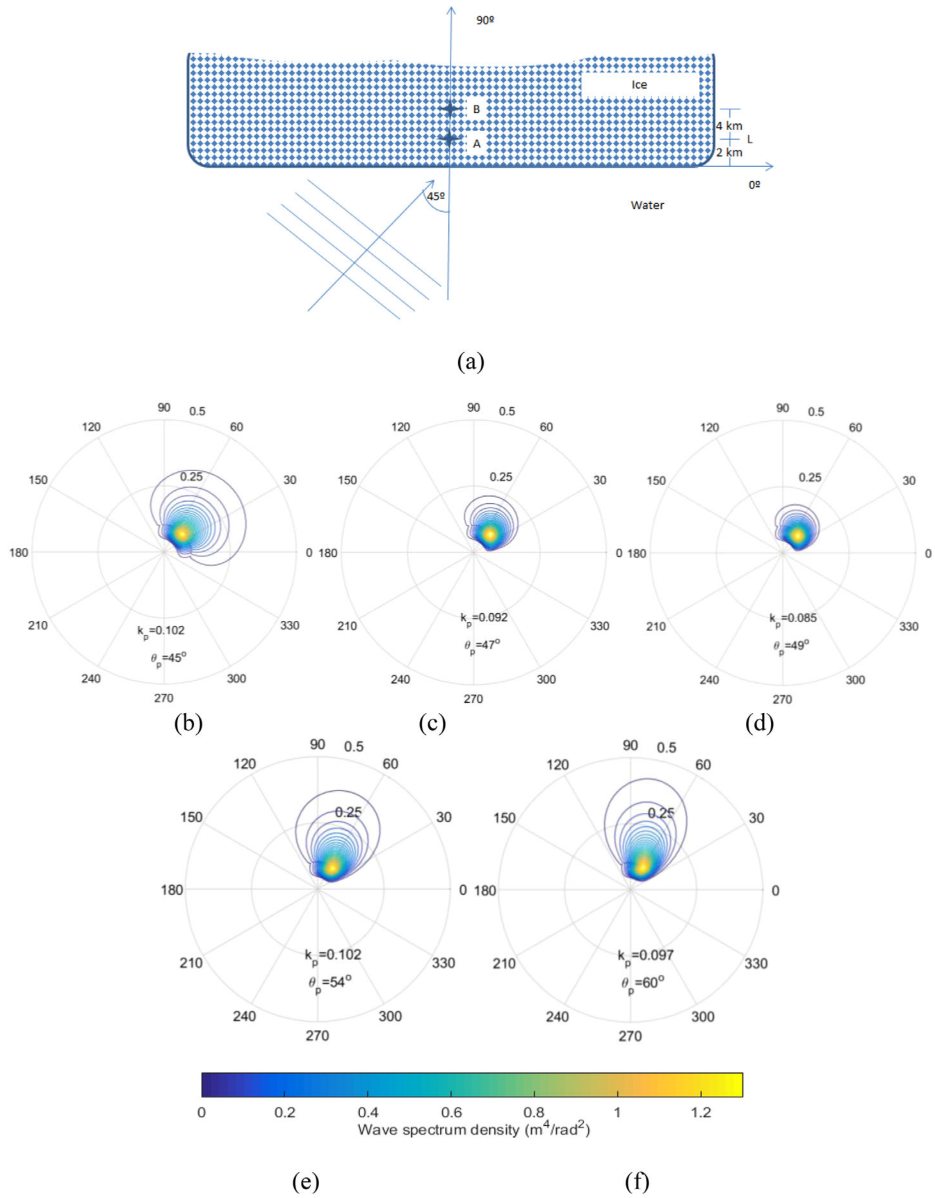

Figure 6. Simulation of waves propagating in the MIZ based on viscous layer theory. (a) Schematic plot of a wave-ice system; (b) directional wave spectrum for incoming waves from open water; simulated wave spectrums in MIZ at (c) 2 km and (d) 4 km from the ice edge; simulated wave spectra with wavenumber independent attenuation coefficient at (e) 2 km and (f) 4 km.

depends on properties of incident waves and on associated ice properties, such as ice concentration, floe size and thickness. These properties are also important in wave-ice scattering models.

3.3.2. Scattering Model

Another mechanism that is generally used to interpret wave attenuation in the MIZ is wave scattering due to sea ice floes (e.g., Perrie & Hu, 1996). We apply the wave scattering model following Kohout and Meylan (2008) with mean floe size parameterization from Dumont et al. (2011) to illustrate wave attenuation in the MIZ as observed by SAR imagery.

The dimensional amplitude attenuation coefficient from wave scattering theory is:

$$\alpha = c\frac{a}{2\bar{D}}$$

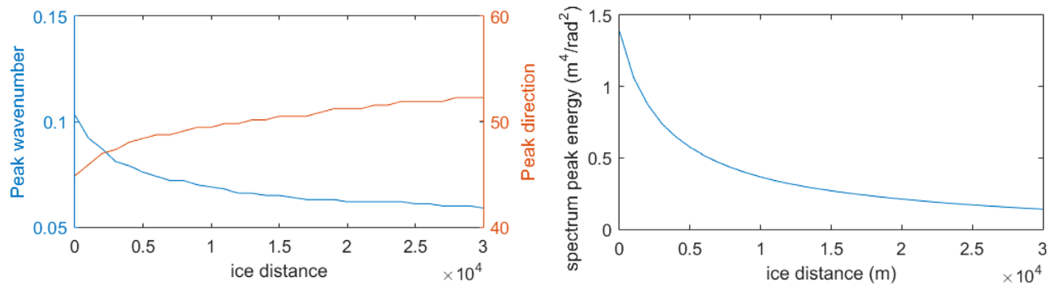

Figure 7. Wave attenuation pattern in the MIZ as simulated by the scattering model of Kohout and Meylan (2008): (a) wavelength and direction, (b) peak spectrum energy.

where α is the attenuation coefficient, c is ice concentration, $\overline{D}$ is the mean size of the floes over the distance traveled by the waves, a is the dimensionless energy attenuation coefficient obtained from a numerical solution of the wave scattering model of Kohout and Meylan (2008). The method to determine $\overline{D}$ is introduced by Dumont et al. (2011). Here, we follow their MIZ calculation to estimate $\overline{D}$ as 36 m in this simulation.

As a first attempt, we assume that the ice concentration c is 50% and ice thickness, 0.6 m, using the same ice – water configuration as shown in Figure 6a and the same incident wave spectrum as for the viscous layer model. Figure 7 shows the resulting wave energy spectrum, indicating the spectral wavelength and direction for the peak energy, for MIZ positions up to 30 km from the ice edge. As shown in Figure 7, as waves propagate into the MIZ, the wave direction tends to shift toward the direction normal (90°) to the ice edge and the wavelength/wavenumber increases/decreases. Changes in the wavelength and direction appear to decrease, as waves propagate further into the MIZ, and relatively shorter waves are further dissipated.

Therefore, we suggest that the wave scattering patterns for wavelengths and directions shown in SAR images can be used to formulate an inverse problem, whereby we may estimate ice floe characteristics in the MIZ, by iterating the numerical simulations with different ice parameters to find the best-fit to the SAR derived evolving wave features (wavelength changes and direction shift etc.), as previously suggested by Meylan and Squire (1993). However, we do not attempt to retrieve these parameters here, due to the lack of in situ data for validation.

3.3.3. Model Validation Against SAR Observations

Both the viscous layer model and the scattering model (introduced in sections 3.3.1 and 3.3.2) take advantage of the attenuation coefficient and the fetch in the MIZ to simulate the wave energy attenuation within MIZ ice. We examine the detailed spectral changes within MIZ ice by adopting two ice conditions. The effective viscous attenuation coefficient is taken from Sutherland and Gascard (2016), based on fitting the viscous layer model to Lidar – measured wave spectra off Greenland; the scattering attenuation coefficient is based on the mean floe size parameterization from (Dumont et al., 2011) together with assumed an ice concentration of 50% and ice thickness of 0.6 m. Based on these two conditions, the wave attenuation in the marginal ice zone is studied by these two models.

As shown in Figures 6 and 7a, both models clearly suggest increasing wavelengths when waves travel from open water into the MIZ ice, with shifting of dominant wave directions when incident wave crests are not parallel to the MIZ ice edge. To this end, the models are sufficiently good that they are able to *qualitatively* explain the wavelength changes and directional shifts in the MIZ as seen in SAR imagery.

For *quantitative* analysis, the in situ ice conditions need to be known, which we unfortunately lack. For the ice conditions from Sutherland and Gascard (2016), the models predict 1°/km direction shift when waves travel into ice with 45° incident angle. Figures 5a an 5b show a direction shift of 14° from ice and water. Considering the MIZ ice fetch of 6.25 km, SAR observes a directional shift of 14°/6.25 km = 2.24°/km. This is about twice the result obtained from the viscous layer model. This difference suggests that the ice conditions studied by Sutherland and Gascard (2016) in northern Greenland might be different to what we have assumed here. By adjusting the effective viscosity coefficient to be double of the value used in Sutherland and Gascard (2016), we can obtain a direction shift of 2°/km, which is close to the SAR observations.

For the scattering model, the model predicts a direction shift of 1°/km (Figure 7a). This is also about half of the rate that is observed by SAR imagery. By changing the ice thickness to 1.2 m, the scattering model

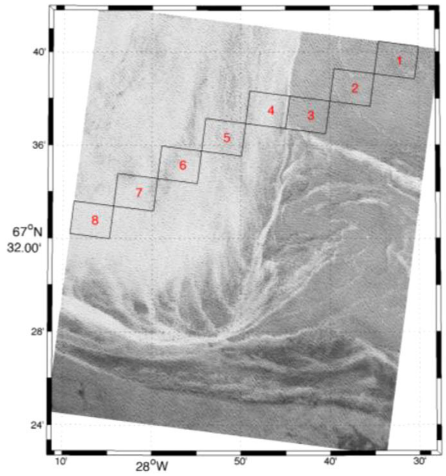

(a)

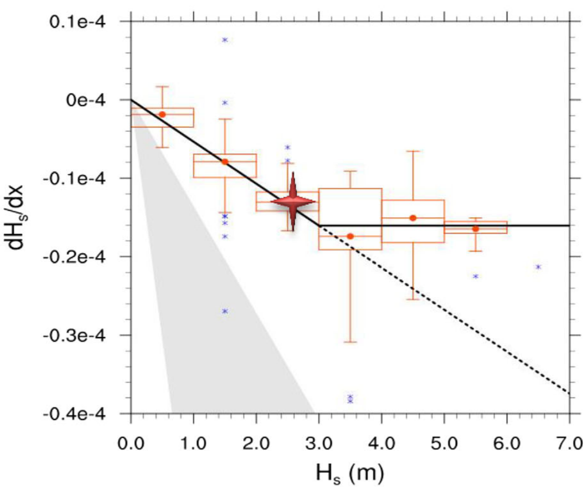

(b)

Figure 8. Wave attenuation analysis from the quad-pol Radarsat-2 SAR image: (a) The quad-pol SAR image with selected sub-image boxes superimposed, with box size 512 × 512 pixels (~2.5 km × 3.2 km); (b) Retrieved rate of change in significant wave height as waves propagate into the MIZ, showing attenuation rate retrieved from SAR, indicated by symbol ✦, overlaid on results from field measurements of Kohout et al. (2014) showing wave height decay more than 100 km from the Antarctic Ocean ice edge. Data are binned in 1-m boxes, with median shown by red dot. Black line is linear least-squares regression through median values.

predicts a directional shift of 2°/km. In this way, the scattering model also can correctly predict the direction shift observed by the SAR imagery. Therefore, both models can predict the wave changes correctly, by adapting the attenuation coefficient and assuming appropriate ice conditions.

To further develop and validate the models, future remotely sensed SAR observations should coordinate with joint in situ programs to measure the wave and ice conditions. Thus, SAR may be used to retrieve ice conditions and investigate wave changes in MIZ ice based on the model validation methodology presented here.

3.4. Wave Attenuation Rate Retrieved From Quad-Pol SAR Images

A series of quad-pol RADARSAT-2 SAR images were also obtained during the time between 08:03:25 and 08:03:34 UTC, which is 12 hours earlier than the ScanSAR image presented in sections 3.1 and 3.2. ECMWF reanalysis data show that the wave patterns in the vicinity of the studied area remain relatively stable, with the pure swell system propagating from south to north, into the marginal ice zone (Figures 2 and 8). The wave stripe patterns in SAR imagery are clearly evident, within both the MIZ ice zone and the water area; thus we can demonstrate the ability of the swell to penetrate through the MIZ ice before traveling back into the open water. The associated wave slope spectra and wave heights can be retrieved from the quad-pol SAR images following the methodology of He et al. (2006) and Zhang et al. (2010).

A sequence of sub-images from the quad-pol SAR image along the wave direction was selected for analysis, extending from open water, into the MIZ (Figure 8a). Because the waves are relatively long and the patches of ice are expected to be thin, we assume that the same relationship between wave slope and the full polarization radar return signals applies in the MIZ as for the open ocean, following Vachon et al. (1993) and Schulz-Stellenfleth and Lehner (2002). Thus, we obtain estimates for the corresponding waves. As the waves travel through the MIZ ice floes, the wave amplitudes are attenuated. In this case, based on the retrieved wave heights from SAR images, for waves within the MIZ, the rate of wave attenuation is about 1.8~3.7% energy loss for every 2.5 km box length on the MIZ transect. In terms of dissipation rate and wave heights, the average dissipation rate is $-0.13e^{-4}$ for dH_s/dx, for incident wave heights of 2.6 m as derived from boxes #4 to #8 in Figure 8a. This result is comparable to recent in situ measurements in the Southern Ocean by Kohout et al. (2014), shown in Figure 8b.

4. Discussion and Conclusions

When waves propagate from open water to the MIZ, high frequency and middle-frequency waves tend to be dampened, transferring their energy to the motions of ice floes, following Meylan and Masson (2006). The remaining portion of the wave spectrum, consisting of long-period waves, tends to penetrate far into the MIZ, and may continue through the area characterized by MIZ ice floes into open water again, depending on the extent of the MIZ area and related ice floe properties like ice floe diameters, thickness, concentration, ice floe position within the MIZ relative to the ice edge and wave spectra parameters, like wave age and frequency. Observations from remotely sensed and in situ field measurements suggest that only the low frequency waves can penetrate relatively far into the MIZ and the attenuation rate increases with frequency.

Within the MIZ ice zone, the wavelength changes are explained by two wave attenuation models taking into account the effects of the ice. Thus, the potentially significant role of wave-ice interactions is confirmed both for present climate conditions, as well as for future climate conditions, predicting continued sea ice retreat in Arctic and possibly enhanced MIZ areas. Gebhardt et al. (2016) studied wavelength changes for waves traveling along a distance of $\sim$1,000 km, for the same storm system as we have considered here. They found that the wavelength changes observed by TerraSAR-X imagery are consistent with the spatial dispersion that is experienced by deep water waves in the open ocean. Moreover, their paper also suggests that in the MIZ ice zone, "the strongest increase was obtained (their image 5). Possibly, the open-water increase of wavelength was enhanced by wave-ice-interaction." Our present paper addresses these wave-ice interaction effects, in terms of their possible contribution to wavelength changes on the relatively local (meso-scale) spatial scale, thus complementing their paper.

In the present study, the wave retrieval methodology for SAR images in the MIZ assumes that ice floes and ice frazil material are approximately homogenously distributed within sub-images. The average wave dissipation rate is $-0.13e^{-4}$ for dH_s/dx, which is consistent with in situ measurements by Kohout et al. (2014). Validation for other types of sea ice in the MIZ requires further study.

The methodology presented here is potentially an important new application of *fully polarimetric* SAR in wave studies in the MIZ, in terms of monitoring waves and ice in the MIZ, by presenting MIZ properties in the spatial domain. By comparison, in situ buoys can give time series data, e.g., the temporal domain, at point locations. Until now, modelers have had to rely on a limited number of measurements of wave attenuation from field measurements; the potential of fully polarimetric SAR imagery was not explored. Even if all the in situ field projects planned in the next few years are successful, they can only provide measurements of attenuation at a handful of new in situ MIZ locations. In situ field experiments are costly and difficult. By comparison, SAR is ubiquitous for its ability to retrieve wave spectrum and ice conditions simultaneously, at high resolution in almost all-weather conditions.

Recent studies (Meylan et al., 2014) based on the in situ experiment of Kohout et al. (2014) suggest that the wave attenuation is proportional to wavenumber. A specifically designed experiment for a series of quad-pol SAR images extending hundreds of kilometers along the wave propagation direction under high wave conditions might be able to investigate this process.

We have demonstrated that high resolution satellite remote sensing measurements from fully polarimetric SAR can provide some elucidation of the characteristics of waves as they propagate into the MIZ. These measurements provide wave information in the spatial domain, whereas in situ measurements are able to give details in the temporal domain. The combination of spatial and temporal information is able to give a more complete picture of the manner in which waves propagate through the MIZ. Clearly, combinations of simultaneous measurements from satellites and in situ measurements from wave buoys are recommended for MIZ studies of ocean waves.

Acknowledgments
The RADARSAT-2 SAR data are provided by Canadian Space Agency (CSA), MODIS L1B data are from http://ladsweb.nascom.nasa.gov/, ASCAT data from Remote Sensing Systems http://www.remss.com/missions/ascat, Jason-2 data from GlobWave http://globwave.ifremer.fr/, ECMWF data from https://www.ecmwf.int, CMC data are from Environment Canada https://weather.gc.ca/model_forecast/. The present work is supported by CSA's Government Research Initiatives Program (GRIP) on wave-ice interactions, by the Office of Energy R & D (PERD), by the Office of Naval Research (ONR) initiative on Sea State and Boundary Layer Physics of the Emerging Arctic Ocean (N00014-15-1-2611), and National Natural Science Foundation(41620104003 and 4177619).

References

Alpers, W. R., Ross, D. B., & Rufenach, C. L. (1981). On the detectability of ocean surface waves by real and synthetic aperture radar. *Journal of Geophysical Research*, *86*, 6481–6498.
Ardhuin, F., Stopa, J., Chapron, B., Collard, F., Smith, M., Thomson, J., . . . Wadhams, P. (2017). Measuring ocean waves in sea ice using SAR imagery: A quasi-deterministic approach evaluated with Sentinel-1 and in situ data. *Remote Sensing of Environment*, *189*, 211–222.
Bendat, J. S., & Piersol, A. G. (1971). *Measurement and analysis of random data*. New York, NY: John Wiley.
Brüning, C., Schmidt, R., & Alpers, W. (1994). Estimation of the ocean wave-radar modulation transfer function from synthetic aperture radar imagery. *Journal of Geophysical Research*, *99*, 9803–9815.
Cheng, S., Rogers, W. E., Thomson, J., Smith, M., Doble, M., Wadhams, P., . . . Shen, H. H. (2017). Calibrating a viscoelastic sea ice model for wave propagation in the Arctic Fall marginal ice zone. *Journal of Geophysical Research: Oceans*, *122*, 8770–8793. https://doi.org/10.1002/2017JC013275
Collins, C. O., III, Rogers, W. E., Marchenko, A., & Babanin, A. V. (2015). In situ measurements of an energetic wave event in the Arctic marginal ice zone. *Geophysical Research Letters*, *42*, 1863–1870. https://doi.org/10.1002/2015GL063063.
Doble, M. J., & Bidlot, J. (2013). Wave buoy measurements at the Antarctic sea ice edge compared with an enhanced ECMWF WAM: Progress towards global waves-in-ice modelling. *Ocean Modelling*, *70*, 166–173.
Donelan, M. A., Hamilton, J., & Hui, W. H. (1985). Directional spectra of wind-generated waves. *Philosophical Transactions of the Royal Society A: Mathematical, Physical and Engineering Sciences*, *315*, 509–562.
Dumont, D., Kohout, A., & Bertino, L. (2011). A wave-based model for the marginal ice zone including a floe breaking parameterization. *Journal of Geophysical Research*, *116*, C04001. https://doi.org/10.1029/2010JC006682
Gebhardt, C., Bidlot, J. R., Gemmrich, J., Lehner, S., Plekachevsky, A., & Rosenthal, W. (2016). Wave observation in the marginal ice zone with the TerraSAR-X satellite. *Ocean Dynamics*, *66*, 839–852.
Hasselmann, K., Raney, R. K., Plant, W. J., Alpers, W., Shuchman, R. A., Lyzenga, D. R., . . . Tucker, M. J. (1985). Theory of synthetic aperture radar ocean imaging; A MARSEN view. *Journal of Geophysical Research*, *90*, 4659–4686.
He, Y., Shen, H., & Perrie, W. (2006). Remote sensing of ocean waves by polarimetric SAR. *Journal of Atmospheric and Oceanic Technology*, *23*, 1768–1773. https://doi.org/10.1175/JTECH1948.1

Khon, V. C., Mokhov, I. I., Pogarskiy, F. A., Babanin, A., Dethloff, K., Rinke, A., & Matthes, H. (2014). Wave heights in the 21st century Arctic Ocean simulated with a regional climate model. *Geophysical Research Letters*, *41*, 2956–2961. https://doi.org/10.1002/2014GL059847

Kohout, A. L., & Meylan, M. H. (2008). An elastic plate model for wave attenuation and ice floe breaking in the marginal ice zone. *Journal of Geophysial Research*, *113*, C09016. https://doi.org/10.1029/2007JC004434

Kohout, A. L., Williams, M. J. M., Dean, S., & Meylan, M. H. (2014). Storm-induced sea ice breakup and the implications for ice extent. *Nature*, *509*, 604–607. https://doi.org/10.1038/nature13262.

Kohout, A. L., Williams, M. J. M., Toyota, T., Lieser, J., & Hutchings, J. (2016). In situ observations of wave-induced sea ice breakup. *Deep Sea Research Part II: Topical Studies in Oceanography*, *131*, 22–27.

Lee, C. M., Cole, S., Doble, M., Freitag, L., Hwang, P., Jayne, S., . . . Zhang, J. (2012). Marginal Ice Zone (MIZ) Program: Science and experiment plan (Tech. Rep. APL-UW 1201, 48 pp.). Seattle, WA: Applied Physics Laboratory, University of Washington.

Liu, A. K., & Mollo-Christensen, E. (1988). Wave propagation in a solid ice pack. *Journal of Physical Oceanography*, *18*(11), 1702–1712.

Liu, A. K., Vachon, P. W., Peng, C. Y., & Bhogal, A. S. (1992). Wave attenuation in the marginal ice zone during LIMEX. *Atmosphere-Ocean*, *30*(2), 192–206.

Masson, D., & LeBlond, P. (1989). Spectral evolution of wind-generated surface gravity waves in a dispersed ice field. *Journal of Fluid Mechanics*, *202*, 111–136.

Meylan, M., Bennetts, L. G., & Kohout, A. L. (2014). In situ measurements and analysis of ocean waves in the Antarctic marginal ice zone. *Geophysical Research Letters*, *41*, 5046–5051. https://doi.org/10.1002/2014GL060809

Meylan, M. H., & Masson, D. (2006). A Linear Boltzmann Equation to model wave scattering in the marginal ice zone. *Ocean Modelling*, *11*(3–4), 417–427.

Meylan, M., & Squire V. A. (1993). Finite-floe wave reflection and transmission coefficients from a semi-infinite mode. *Journal of Geophysical Research: Oceans*, *98*(C7), 12537–12542. https://doi.org/10.1029/93JC00940

Montiel, F., & Squire, V. A. (2017). Modelling wave-induced sea ice break-up in the marginal ice zone. *Proceedings of Royal Society A*, *473*, 20170258. https://doi.org/10.1098/rspa.2017.0258

Montiel, F., Squire, V. A., & Bennetts, L. G. (2016). Attenuation and directional spreading of ocean wave spectra in the marginal ice zone. *Journal of Fluid Mechanics*, *790*, 492–522.

Perrie, W., & Hu, Y. (1996). Air-ice-ocean momentum exchange. Part 1: Energy transfer between waves and ice floes. *Journal of Physical Oceanography*, *26*(9), 1705–1720.

Pierson, W. J., & Moskowitz, L. (1964). A proposed spectral form for fully developed wind seas based on the similarity theory of S. A. Kitaigorodskii. *Journal of Geophysical Research*, *69*, 5181–5190.

Rogers, E. W., Thomson, J., Shen, H. H., Doble, M. J., Wadhams, P., & Cheng, S. (2016). Dissipation of wind waves by pancake and frazil ice in the autumn Beaufort Sea. *Journal of Geophysical Research: Oceans*, *121*, 7991–8007. https://doi.org/10.1002/2016JC012251

Schulz-Stellenfleth, J., & Lehner, S. (2002). Spaceborne synthetic aperture radar observations of ocean waves traveling into sea ice. *Journal of Geophysical Research*, *107*(C8), 3106. https://doi.org/10.1029/2001JC000837

Squire, V. A., & Montiel, F. (2016). Evolution of directional wave spectra in the marginal ice zone: A new model tested with legacy data. *Journal of Physical Oceanography*, *46*, 3121–3137.

Stopa, J. E., Ardhuin, F., & Girard-Ardhuin, F. (2016). Wave climate in the arctic 1992–2014: Seasonality and trends. *The Cryosphere*, *10*, 1605–1629.

Sutherland, P., & Gascard, J.-C. (2016). Airborne remote sensing of ocean wave directional wavenumber spectra in the marginal ice zone. *Geophysical Research Letters*, *43*, 5151–5159. https://doi.org/10.1002/2016GL067713

Thomson, J., & Rogers, W. E. (2014). Swell and sea in the emerging Arctic Ocean. *Geophysical Research Letters*, *41*, 3136–3140. https://doi.org/10.1002/2014GL059983

Thomson, J., Squire, V., Ackley, S., Rogers, E., Babanin, A., Guest, P., . . . Bidlot, J. (2013). Sea state and boundary layer physics of the emerging Arctic Ocean (Tech. Rep. APL-UW TR1306, 61 p.). Retrieved from http://www.apl.washington.edu/research/downloads/publications/tr_1306.pdf

Toffoli, A., Bennetts, L. G., Meylan, M. H., Cavaliere, C., Alberello, A., Elsnab, J., & Monty, J. P. (2015). Sea ice floes dissipate the energy of steep ocean waves. *Geophysical Research Letters*, *42*, 8547–8554. https://doi.org/10.1002/2015GL065937

Tolman, H. L. (2009). User manual and system documentation of WAVEWATCH III version 3.14 (Tech. Note 276, 194 pp.). NOAA/NWS/NCEP/MMAB.

Vachon, P. W., Olsen, R. B., Krogstad, H. E., & Liu, A. K. (1993). Airborne synthetic aperture radar observations and simulations for waves in ice. *Journal of Geophysical Research*, *98*, 16411–16425. https://doi.org/10.1029/93JC00914

Wadhams, P. (1986). The seasonal ice zone. In: N. Untersteiner (Ed.) *The geophysics of sea ice* (pp. 825–991). New York: Plenum Pub. Corp.

Wadhams, P., Parmiggiani, F., & de Carolis, G. (2002). The use of SAR to measure ocean wave dispersion in Frazil-Pancake Ice fields. *Journal of Physical Oceanography*, *32*, 1721–1746.

Wadhams, P., Squire, V. A., Goodman, D. J., Cowan, A. M., & Moore, S. C. (1988). The attenuation rates of ocean waves in the marginal ice zone. *Journal of Geophysical Research*, *93*, 6799–6818.

Wang, M., & Overland, J. E. (2009). A sea ice free summer Arctic within 30 years? *Geophysical Research Letters*, *36*, L07502. https://doi.org/10.1029/2009GL037820

Williams, T. D., Bennetts, L. G., Squire, V. A., Dumont, D., & Bertino, L. (2013a). Wave-ice interactions in the marginal ice zone. part 1: Theoretical foundations. *Ocean Modelling*, *70*, 81–91.

Williams, T. D., Bennetts, L. G., Squire, V. A., Dumont, D., & Bertino, L. (2013b). Wave-ice interactions in the marginal ice zone. part 2: Numerical implementation and sensitivity studies along 1d transects of the ocean surface. *Ocean Modelling*, *71*, 92–101.

Zhang, B., Perrie, W., & He, Y. (2010). Validation of RADARSAT-2 fully polarimetric SAR measurements of ocean surface waves. *Journal of Geophysical Research*, *115*, C06031. https://doi.org/10.1029/2009JC005887